Chinese Chemical Letters 37 (2026) 112064

Contents lists available at ScienceDirect

Chinese Chemical Letters

journal homepage: www.elsevier.com/locate/cclet

Development of visible-light photocaged molecular glues (vc-MGs) for B-cell malignancies therapy with improved safety and pharmacokinetic profiles *in vivo*

Wei Yan[a,b,1], Naizhen Zhang[a,b,1], Xiao Liu[a,b,1], Qiyu He[a,b], Xucheng Lv[a], Jianghui Sun[a,b], Lili Zhuang[a,b], Yuexin Zou[a,b], Yajie Zhang[a,b], Yuhang Liang[a], Yanjie Wang[a], Siyuan Li[a], Yonghui Sun[a,b,*]

[a] *State Key Laboratory of Bioactive Substance and Function of Natural Medicines, Institute of Materia Medica, Chinese Academy of Medical Sciences & Peking Union Medical College, Beijing 100050, China*
[b] *Beijing Key Laboratory of Active Substance Discovery and Druggability Evaluation, Institute of Materia Medica, Chinese Academy of Medical Sciences & Peking Union Medical College, Beijing 100050, China*

ARTICLE INFO

Article history:
Received 9 September 2025
Revised 3 November 2025
Accepted 4 November 2025
Available online 5 November 2025

Keywords:
Molecular glues
Visible-light photocage
Burkitt's lymphoma
General toxicity
Druggability

ABSTRACT

Molecular glues (MGs) represent a promising approach in protein regulation, especially for "undruggable" targets. Despite the advantages over traditional protein inhibitors and proteolysis-targeting chimeras (PROTACs), MGs show various off-target effects, inducing general toxicities in patients. Herein, we describe a structure-guided design of visible-light photocaged MGs (vc-MGs), which precisely and spatiotemporally control the G1 to S phase transition 1 (GSPT1) protein level and Burkitt's lymphoma through visible-light irradiation *in vitro* and *in vivo*. Notably, activated VL-MG-9 showed a potent antitumor effect in the RAMOS xenograft mouse model, while VL-MG-9 alone has no GSPT1 degradation activity or general toxicity in various organs even at high dose. Furthermore, proteomics assay and apoptosis analysis confirmed the selectivity and safety of VL-MG-9. Significantly, pharmacokinetic results demonstrated the enhanced permeability and bioavailability (*F*%) of VL-MG-9. These data clearly reveal the practicality and importance of vc-MGs as preliminary tool for the targeted therapy of malignancies with reduced systemic toxicity and improved druggability.

© 2026 Published by Elsevier B.V. on behalf of Chinese Chemical Society and Institute of Materia Medica, Chinese Academy of Medical Sciences.

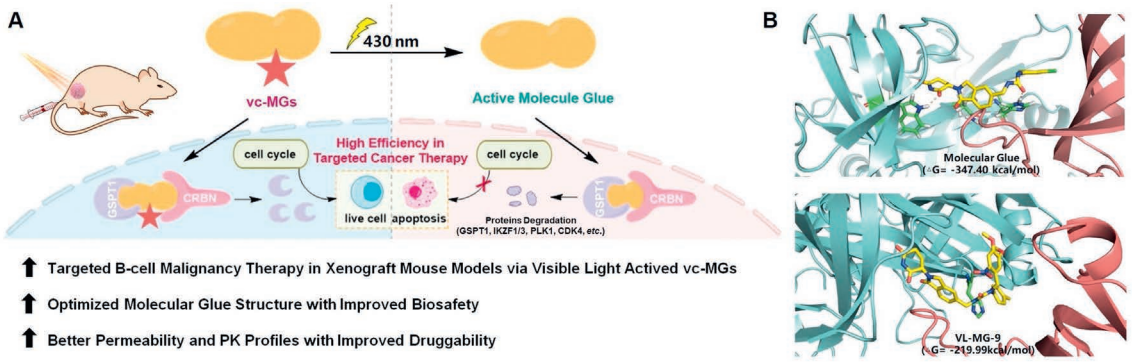
Burkitt's lymphoma (BL) is a highly aggressive B-cell malignancy in children and adults [1,2]. As the most common type of non-Hodgkin lymphoma (NHL) in adolescents, BL accounts for ~50% of NHL cases, with an estimated 30,000 people worldwide being diagnosed with BL each year [3–5]. BL is always accompanied by chromosomal translocation, which increases the difficulty in overcoming BL [6]. Moreover, current chemotherapy for refractory BL always leads to relapse, and the incidence of treatment failure is as high as 35% [7–9]. Additionally, chemotherapy-induced toxicity limits patient compliance [10–12]. These statistics highlight an urgent need to develop more effective therapeutic strategies for patients with BL.

Molecular glues (MGs) represent a novel class of proximity-inducing small molecules [13–16], that adjoin an E3 ligase (*e.g.*, cereblon (CRBN), von Hippel-Lindau (VHL)) with heterologous target proteins to establish complementarity on the surface [17–19]. Although PROTAC has achieved remarkable breakthroughs [20,21], MGs display advantages of improved anti-cancer efficiency, less resistance, and the ability to target "undruggable" pathways [22–24]. However, off-target toxicity hinders the broader implementation of MG-based therapies [22,25]. Additionally, the mechanism of off-target phenomena has not yet been clearly defined [26]. CRBN-based MGs are newly developed compounds with potent anticancer activity. However, some of the CRBN-based MGs, such as thalidomide and CC-885, always have multiple targets with unmanageable toxicities *in vivo* [27–29]. Moreover, some of the CRBN-based MGs contain thalidomide-based ligands, which lead to serious off-target effects and result in pronounced clinical toxicity, such as congenital anomalies [30,31].

CC-885, an analog of lenalidomide, is a typical CRBN-based MG with potent antitumor activity. CC-885 has been proven to mediate the binding of the translation termination factor G1 to S phase transition 1 (GSPT1) to $CRL4^{CRBN}$ (PDB: 5HXB), inducing the degra-

* Corresponding author.
E-mail address: sunyonghui@imm.ac.cn (Y. Sun).
[1] These authors contributed equally to this work.

https://doi.org/10.1016/j.cclet.2025.112064
1001-8417/© 2026 Published by Elsevier B.V. on behalf of Chinese Chemical Society and Institute of Materia Medica, Chinese Academy of Medical Sciences.

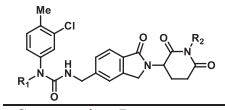


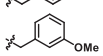
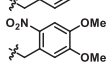
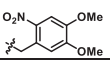
Scheme 1. Schematic representation and characterization of vc-MGs. (A) Brief illustration and mechanism of the newly developed vc-MGs. (B) Molecular dynamics of the binding of compound VL-MG-9 with GSPT1 and CRBN. GSPT1-CRBN complex with CC-885 was used (PDB code: 5HXB).

dation of the target protein GSPT1. The half-maximal inhibitory concentration (IC_{50}) values of CC-885 for the proliferation of AML cell lines were lower than 10 nmol/L [32]. However, recent research has confirmed that CC-885 promotes tumor cell death by targeting diverse proteins (*e.g.*, GSPT1, polo-like kinase 1 (PLK1), casein kinase 1 alpha (CK1α), cyclin-dependent kinase 4 (CDK4) and HBS1 like translational GTPase (HBS1L)) for ubiquitin-dependent degradation [26,28,33]. CC-885 showed general toxicity to normal cells, such as myoblasts and fibroblasts from an unaffected individual, with an IC_{50} of ~20 nmol/L [34]. The clinical development of CC-885 has been hampered by significant toxicity [35]. Therefore, it is critically important to develop novel therapeutic strategies for controlling MGs to achieve precise antitumor effects. Although light-controlled release has been the Holy Grail of drug design [36,37], the control of MGs with visible-light *in vivo* has not yet been achieved. In addition, compared with UV light, visible light has distinctly lower phototoxic effects and photochemical damage [38–40].

Herein, we describe our discovery of visible-light photocaged MGs (vc-MGs), which precisely and spatiotemporally controlled protein degradation and tumor growth through visible light in a mouse B-cell malignancy xenograft model. Remarkably, the representative compound of vc-MGs, VL-MG-9, efficiently degraded GSPT1 and inhibited the growth of BL under irradiation by visible light *in vivo*. Additionally, unlike CC-885, VL-MG-9 exhibited no protein degradation activity or general toxicity in various mouse organs even at high dose. Moreover, quantitative proteomics experiments and histopathological analysis *in vivo* demonstrated the safety of VL-MG-9. More importantly, the pharmacokinetic (PK) results confirmed the improved bioavailability and druggability of VL-MG-9, indicating the strong potential for the development of visible-light photocaged MGs with broad clinical application prospects (Scheme 1A).

Table 1
Photochemical properties and bioactivities of vc-MGs.



Compound	R_1	R_2	Degradation blocking (%)[a]	$T_{1/2}$ (min)[b]
VL-MG-1		H	87.7 ± 7.8	>30.0
VL-MG-3		H	30.9 ± 8.3	-[c]
VL-MG-4		H	10.6 ± 2.0	-[c]
VL-MG-6		H	84.5 ± 7.9	19.7 ± 2.5
VL-MG-7		H	74.6 ± 7.5	7.4 ± 2.7
VL-MG-9		H	95.6 ± 7.9	4.3 ± 2.0
VL-MG-10	H		78.0 ± 4.5	>30.0

[a]Relative GSPT1 protein level after treatment of RAMOS cell line with 33 nmol/L the indicated compounds. The degradation blocking referred to the ratio of GSPT1 level in 33 nmol/L compound group compared to GSPT1 level in DMSO group.
[b]Photolysis half-life of vc-MGs under 430 nm light irradiation. RAMOS cells were treated with compounds at 33 nmol/L concentration (under 430 nm light irradiation), the protein levels of GSPT1 at different irradiation times were utilized to calculate the half-life of vc-MGs.
[c]Not applicable because of the low degradation blocking values. All the values were means from three replicates.

To develop visible-light photocaged MGs, various kinds of photo-control groups were conjugated to the degradation arm, a structural unit that binds to the E3 ligase and acts as a degradation machinery-recruiting unit [41]. Photo-control groups serve to hinder the formation of the GSPT1-MG-CRBN complex (Table 1). According to the cocrystal structure (PDB: 5HXB). The nitrogen atoms of the urea moiety in CC-885 form hydrogen bonds with the carboxyl group of Glu377 in CRBN protein. Additionally, the carbonyl group of the urea moiety engages in a hydrogen bond with the imidazole ring of His353. This interaction demonstrates that attaching a photo-control group to the urea moiety of CC-885 can sterically hinder the interaction between CC-885 and CRBN. Furthermore, the nitrogen atom of the cyclic lactam in CC-885 forms a hydrogen bond with His378, indicating that this site is also suitable for the attachment of a photo-control group to inhibit the bioactivity of CC-885 (Scheme 1B). The photolysis of vc-MGs upon 430 nm irradiation was monitored by the GSPT1 degradation level in RAMOS cell line, which serves as a model of Burkitt's lymphoma. The results revealed that compound VL-MG-9, with a dimethoxy-2-nitrobenzyl group on the urea, moiety demonstrated the best degradation blocking ability and photolysis activity. Moreover, molecular dynamics simulation results confirmed that the photo-control group of VL-MG-9 significantly reduced the binding affinity of GSPT1 for CRBN and then blocked the activity of CC-885 (Scheme 1B).

We also tried to introduce the photosensitive group on the non-aniline nitrogen of the urea moiety to synthesize an isomer of VL-MG-9. The non-aniline urea nitrogen atom is closer to the protein-protein interaction (PPI) interface of the ternary complex according to the cocrystal structure of CRBN–CC885-GSPT1 (PDB: 5HXB). Moreover, this nitrogen atom is situated deeper within the CRBN ligand binding pocket. Therefore, modification with photo-control group at this position is expected to provide more effective steric hindrance to inhibit the bioactivity of CC-885. However, the aniline material failed to transform into a urea moiety, a result that may be due to the poor nucleophilicity of 3–chloro–4-methylaniline.

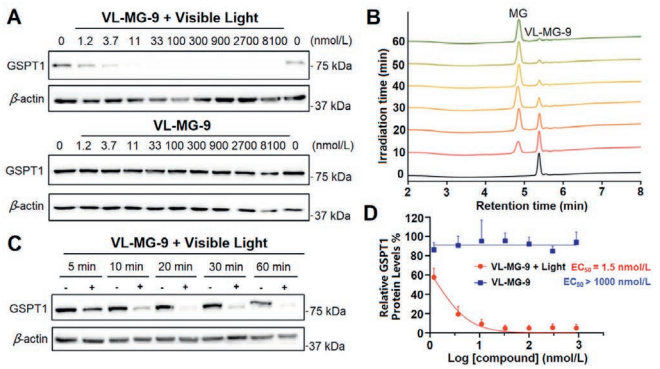


Fig. 1. *In vitro* photo-induced release efficiency and degradation activity of vc-MGs. (A) Degradation activity of VL-MG-9 on GSPT1 protein in RAMOS cell line with or without irradiation of visible light (430 nm for 20 min). (B) HPLC chromatograms of compound VL-MG-9 under the 430 nm irradiation for different times. (C) Results of Western blot assay of GSPT1 levels in RAMOS cell line with VL-MG-9 at various irradiation times. (D) Compared with VL-MG-9, light-activated VL-MG-9 induced GSPT1 degradation in a dose-dependent manner. Data are presented as mean ± standard deviation (SD) ($n = 3$).

Compound CC-885 induces the formation of a tight complex between CRBN and GSPT1 (PPI). The urea group of CC-885 is located at the CRBN-GSPT1 interface. Benzylation of the urea group not only sterically hinders the interaction between CC-885 and CRBN, but also impedes subsequent binding of CRBN-GSPT1, thereby inhibiting CRBN-mediated ubiquitination of GSPT1. Based on the number of hydrogen bonds and the depth of the ligand-binding pocket of CRBN, introducing a photo-control group on the glutarimide moiety is considered the optimal strategy to inhibit the binding of the CC-885. The carbonyl group of the glutarimide forms hydrogen bonds with the imidazole ring and carbonyl group of His378, while the other carbonyl group interacts with the hydroxyl group of Ser379 and the amino group of Trp380. Additionally, the amino group of the glutarimide participates in a hydrogen bond with the carbonyl group of His378. Although the incorporation of the photo-control group through the imide nitrogen of the thalidomide moiety (VL-MG-10) could efficiently hamper the binding and degradation capability of CC-885, it failed to produce an appreciable amount of the major product even after 1 h of irradiation (Figs. S1 and S2 in Supporting information). To investigate the mechanism underlying the poor photolysis of compound VL-MG-10, we experimentally measured UV–vis absorption spectra of VL-MG-9 and VL-MG-10. The results showed that the absorption spectra of VL-MG-9 and VL-MG-10 were similar (Fig. S3 in Supporting information). Furthermore, density functional theory (DFT) calculations were carried out. Compared with VL-MG-9, the energy barrier of the photolysis process of VL-MG-10 was higher, which may lead to its lower photolysis efficiency (Fig. S4 in Supporting information). According to the result, VL-MG-9 exhibited the best performance in both "degradation blocking" and "$T_{1/2}$" tests (Table 1). As the representative compound of vc-MGs, VL-MG-9 rapidly converted to CC-885 under the irradiation of 430 nm light. Therefore, compound VL-MG-9 was selected for subsequent studies.

The photo-induced release efficiency and protein degradation activity of VL-MG-9 were assessed in RAMOS cell line. VL-MG-9 demonstrated significant GSPT1 degradation under irradiation of visible light with a half-maximal degradation concentration (DC_{50}) of 1.5 nmol/L. Without visible light irradiation, VL-MG-9 alone did not induce the degradation of GSPT1 even at high concentrations (Fig. 1A). Moreover, the photolysis efficiency of VL-MG-9 was monitored by high performance liquid chromatography (HPLC). VL-MG-9 solution was prepared in DMSO at a concentration of 50 mmol/L and was irradiated by 430 nm visible light. The results demonstrated that no CC-885 was found *via* HPLC without irradiation. In contrast, ~50 % of VL-MG-9 was converted to CC-885 with light irradiation for 10 min (Fig. 1B).

Moreover, the photolysis efficiency of VL-MG-9 at various irradiation times was also analyzed *via* the degradation of GSPT1 protein. Compared with the control group (no light irradiation), time-dependent GSPT1 degradation was observed under the irradiation of 430 nm light. Indeed, GSPT1 protein degradation began within 5 min. Notably, significant GSPT1 degradation was detected after 20 min of irradiation (Fig. 1C). Furthermore, GSPT1 levels were monitored under different concentrations of VL-MG-9. The result revealed that no protein degradation occurred without light irradiation. Compared with VL-MG-9 as a caged MG, light-activated VL-MG-9 induced GSPT1 degradation in a dose-dependent manner (Fig. 1D).

Anti-malignant activity in Burkitt's lymphoma was further investigated. As shown in Fig. 2A, VL-MG-9 had potent anti-proliferative activity against Burkitt's lymphoma (half-maximal effective concentration (EC_{50}) = 2 nmol/L) with irradiation. However, VL-MG-9 had a much weaker inhibitory effect on cell growth (EC_{50} = 329 nmol/L) without irradiation, indicating that VL-MG-9 has a low toxicity potential. As shown in Fig. S6 (Supporting information), VL-MG-9 increased caspase-3 and poly(ADP-ribose) polymerase 1 (PARP1) cleavage at high concentrations. This result was consistent with the proliferation inhibition effect of VL-MG-9 shown in Fig. 2A. The toxicity of VL-MG-9 may occur through potential non-specific binding and off-target effects of the lenalidomide ligand. Ikaros family zinc finger protein 1/3 (IKZF1/3) are key targets of lenalidomide and pomalidomide in the treatment of hematological cancer [42]. Degradation of IKZF1 and IKZF3 by cereblon E3 ligase modulators disrupts the interferon regulatory factor 4 (IRF4) myelocytomatosis (MYC) oncogenic signaling axis, resulting in the downregulation of key survival signals. This perturbation induces mitochondrial dysfunction and initiates the intrinsic apoptotic pathway, characterized by cytochrome c release, and subsequent cleavage of caspase-3 and PARP-1, ultimately triggering programmed cell death [43]. We used JC-1 to detect the mitochondrial membrane potential in RAMOS cells. As shown in Fig. S7 (Supporting information), green-fluorescent monomers increased significantly in the VL-MG-9 + 430 nm group, indicating that the mitochondrial membrane potential of most cells was significantly reduced. ATP content assay showed that the ATP level in VL-MG-9 + 430 nm light group was significantly lower than that in other groups. To further investigate the controllable anti-cancer effect of VL-MG-9, apoptosis was assessed *via* flow cytometry. The results demonstrated that VL-MG-9, with visible-light irradiation, significantly induced apoptosis of RAMOS cells, whereas uncleaved VL-MG-9 had no apoptotic effect at low concentration. All the values were means from three replicates. Statistical analysis showed that VL-MG-9 + 430 nm light induced more early-stage apoptosis than late-stage apoptosis (Fig. 2C). Moreover, the apoptotic function of VL-MG-9, controlled by visible-light irradiation, was confirmed through calcein acetoxymethyl ester (calcein-AM) and propidium iodide (PI) staining assay (Fig. 2B).

As mentioned above, CC-885 has been reported to have off-target effects. Therefore, cell viability assay was conducted using human 293T cell line and human umbilical vein endothelial cell line (HUVEC). As presented in Figs. 2D and E, compound VL-MG-9 had much lower toxicity than CC-885. Furthermore, a quantitative proteomic analysis was conducted to illuminate the selectivity of VL-MG-9. The results indicated that CC-885 had multiple degradation targets, such as GSPT1, IKZF1/3, PCLAF, RAD51, IGLC2 and UBL5, at concentration of 30 nmol/L. These targets are essential for cell survival and division. Compared with CC-885, VL-MG-9 offered improved specificity and had a much weaker effect on cell protein signaling at the same concentration. Therefore, VL-MG-9 stands

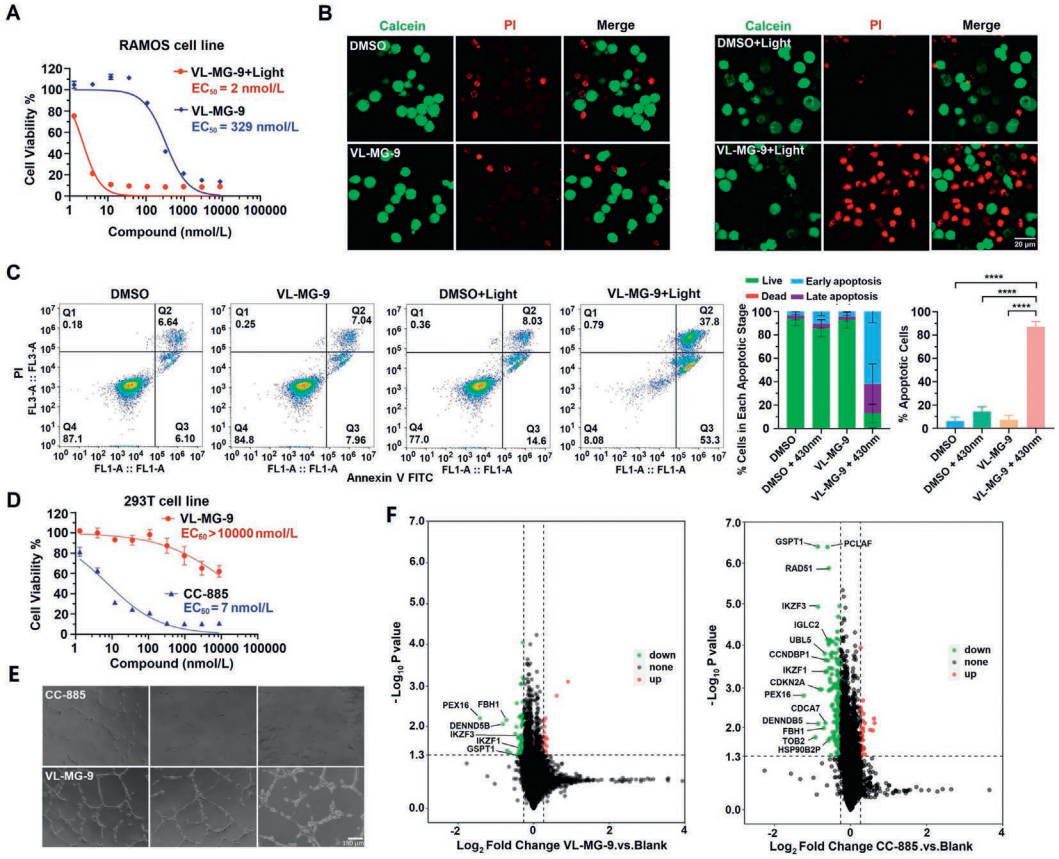


Fig. 2. Anticancer effect, proteomics analysis and general toxicity of vc-MGs upon visible-light radiation *in vitro*. (A) Cell viability of RAMOS cells after treatment with VL-MG-9 or VL-MG-9 + 430 nm light. In 96-well plates, 3000 cells were incubated in each well at 37 °C for 72 h. The final results were calculated using cell counting kit-8 (CCK-8). (B) Calcein-AM/PI staining of RAMOS cells after being treated with VL-MG-9 under different formulations. Scale bar: 20 μm. (C) Flow cytometry quantification of early/late apoptotic cells treated with VL-MG-9 under different formulations. All the values were means from three replicates. Data are expressed as the mean ± standard deviation. $^{****}P < 0.0001$, with two-tailed test for significance. (D) General toxicity test on human 293T cell line. In 96-well plates, 3000 cells were incubated in each well at 37 °C for 72 h. The final EC_{50} was calculated using CCK-8. (E) General toxicity test on human HUVEC cell line with 30 nmol/L indicated compound. Scale bar: 150 μm. (F) Quantitative proteomic analysis. RAMOS cells were treated with 30 nmol/L indicated compound before proteomics measurement. The color coding is defined as follows: green signifies a decrease in protein abundance relative to the negative control; red indicates an increase in protein abundance; and black indicates no significant change in protein levels. Threshold values for $P < 0.05$. Threshold values for fold change > 1.2 or < 0.83. The total protein count was 6425. Three independent biological replicates were performed. Data are presented as mean ± SD ($n = 3$).

out as a novel controllable tool to avoid off-target effects and potential general toxicity. Moreover, combined with irradiation of visible light, VL-MG-9 could be of clinical significance in the precise treatment of cancer (Fig. 2F).

Owing to its potent *in vitro* efficacy, VL-MG-9 was further examined in a mouse xenograft model inoculated with RAMOS cells. All animal experiments were performed under the guidelines, evaluated, and approved by the Ethics Committee of Institute of Materia Medica, Chinese Academy of Medical Sciences and Peking Union Medical College (No. IMM-S-25–0122). Different formulations were injected into the mice, followed by 2 h of visible-light radiation. As shown in Fig. 3A, treatment with VL-MG-9 + 430 nm light resulted in remarkable *in vivo* antitumor effects that were similar to those of CC-885. In contrast, VL-MG-9 or 430 nm light could not independently inhibit tumor growth, which indicated the safety of vc-MGs and visible light. Moreover, systemic toxicity was evaluated by measuring body weight. As shown in Fig. 3B, VL-MG-9 induced nearly no weight loss with or without radiation. Meanwhile, tumors were harvested from different groups of mice after drug treatment (Fig. 3C). Treatment of VL-MG-9 or 430 nm light alone had a slight antitumor effect, which was consistent with the results of tumor weight evaluation (Fig. 3D and Fig. S8 in Supporting information). Relative GSPT1 protein levels in fresh *ex vivo* tumor tissues were also assessed by immunohistochemistry (Fig. 3E). Immunohistochemical staining was performed using a primary antibody against GSPT1, which specifically bound to GSPT1 in the tissue samples. The primary antibody was then coupled to an HRP-conjugated secondary antibody. The complex was subsequently visualized using diaminobenzidine (DAB) chromogen, resulting in a brown precipitate. Hematoxylin, a basic dye, was used as a counterstain to label nucleus (blue). In the VL-MG-9 treatment group, upon light irradiation, VL-MG-9 was converted to CC-885. As a result, both the VL-MG-9 (with light irradiation) and CC-885 treatment groups exhibited a significant reduction in GSPT1 protein levels compared with the negative control group. The reduction in GSPT1 led to a decrease in the intensity of brown DAB staining in these two groups. In contrast, GSPT1 protein levels and brown staining intensity in the other two groups were comparable to those in the negative control group. Additionally, apoptosis-related immunohistochemical markers (cleaved caspase-3 and cleaved PARP1) were evaluated in tumor tissues from differently treated mouse groups (Fig. S9 in Supporting information), the results indicated that VL-MG-9 + light were shown to induce apoptosis *in vivo*.

To further assess the safety of VL-MG-9 *in vivo*, toxicity experiments were conducted in the BALB/c nude mouse model. All the mice in the VL-MG-9-treated groups (120 mg/kg) were in good health. The serum levels of alanine transaminase (ALT) and aspar-

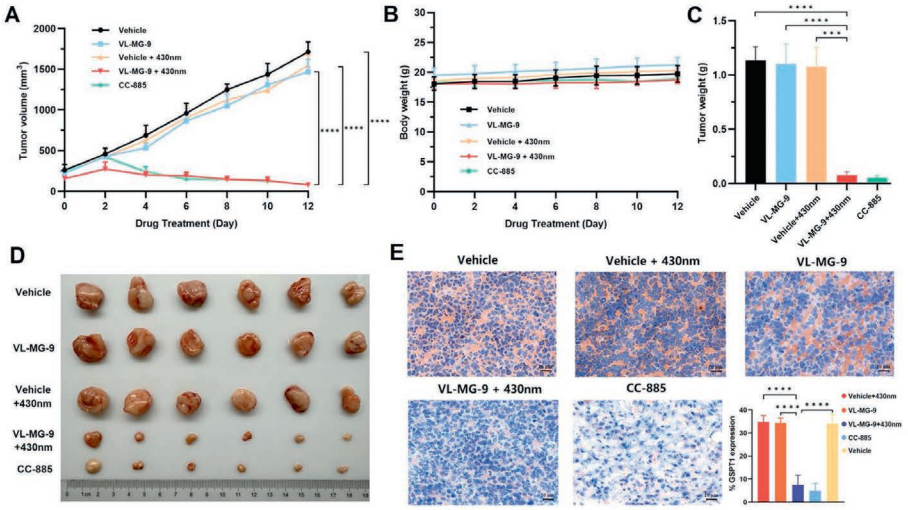
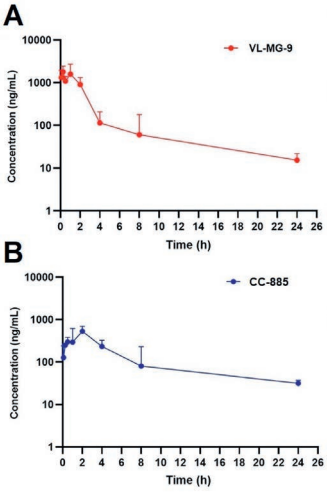


Fig. 3. *In vivo* anticancer efficacy of VL-MG-9 in the RAMOS xenograft mouse model ($n = 6$ mice per group). (A) Tumor growth curves of RAMOS xenograft in nude mice. VL-MG-9 (40 mg/kg), VL-MG-9 (40 mg/kg) + 430 nm light, vehicle, vehicle + 430 nm light, and CC-885 (40 mg/kg) groups. Mice were treated every 2 days once *via* intratumor injection. (B) Minimal changes in the body weight of xenograft mice. (C) Tumor weight on the last day of treatment in different groups. (D) Macroscopic views of xenograft tumors in the different groups after 12 days of the indicated treatments. (E) Immuno-histochemistry results of mice tumor biopsies. Scale bar: 20 μm. Data are expressed as the mean ± SD. $^{****}P < 0.0001$, $^{***}P < 0.001$, with two-tailed test for significance.

tate transaminase (AST) were analyzed. As shown in Fig. S10 (Supporting information), VL-MG-9 exerted nearly no effect on these indicators of liver function in animals with or without visible-light radiation (Fig. S10A); however, CC-885 led to a relatively greater increase, indicating a hepatocellular damage. In order to evaluate the safety profiles of VL-MG-9, the cytotoxicity against normal B lymphocytes was evaluated (Fig. S10B). The results showed that normal B cells were significantly inhibited by CC-885, and the EC_{50} was lower than 1 nmol/L. In contrast, VL-MG-9 had a weak anti-proliferative effect. Moreover, histopathological analysis was performed *via* hematoxylin and eosin (H&E) staining on major organs from the BALB/c mice. As presented in Figs. S10C and D, mice in VL-MG-9 and VL-MG-9 + 430 nm light groups showed no pathological damage. However, mice in CC-885 group exhibited evident pathological alterations in the liver (hepatocellular necrosis) and spleen (sinusoidal dilation and splenomegaly). These results affirm that VL-MG-9 exerts intriguing and potent anti-cancer activity through visible light control and effectively avoids the general toxicity from CC-885 in this BALB/c nude mouse model.

To further elucidate the PK profiles of VL-MG-9, C57BL/6 mice were administered a single dose of VL-MG-9 or CC-885. As shown in Fig. 4 and Fig. S11 (Supporting information), half-life of VL-MG-9 was 6.61 h, slightly lower than that of CC-885 ($t_{1/2} = 7.26$ h). MRT_{inf_obs} is the mean residence time from the first sampled time extrapolated to infinity based on the last observed concentration. The MRT_{inf_obs} of VL-MG-9 was 4.06 h, which was shorter than that of CC-885 ($MRT_{inf_obs} = 8.51$ h). However, compound VL-MG-9 was rapidly absorbed with a higher C_{max} and a shorter T_{max} after administration, indicating that the cage moiety in the structure of VL-MG-9 could improve the absorption property *in vivo*. $AUC_{\%Extrap_obs}$ indicates the percentage of the total area under the curve (AUC) that was extrapolated rather than directly measured from observed data points. As shown in Fig. 4, the $AUC_{\%Extrap_obs}$ values for both VL-MG-9 and CC-885 did not exceed 10 %, demonstrating the accuracy of the AUC values. More importantly, the absolute bioavailability values (*F*%) of VL-MG-9 was ~6-fold greater than that of CC-885. PK data for intravenous administration are presented in Fig. S11. Taken together, these results demonstrate that the cage moiety, as a key ligand employed for visible-light activation, can enhance the PK properties and druggability of vc-MGs.



PK parameters	VL-MG-9
$t_{1/2}$ (h)	6.61
T_{max} (h)	0.250
C_{max} (ng/mL)	1853
AUC_{last} (h*ng/mL)	5129
AUC_{INF_obs} (h*ng/mL)	5282
$AUC_{\%Extrap_obs}$ (%)	2.90
MRT_{INF_obs} (h)	4.06
F%	14.78

PK parameters	CC-885
$t_{1/2}$ (h)	7.26
T_{max} (h)	2.00
C_{max} (ng/mL)	546
AUC_{last} (h*ng/mL)	3444
AUC_{INF_obs} (h*ng/mL)	3781
$AUC_{\%Extrap_obs}$ (%)	8.90
MRT_{INF_obs} (h)	8.51
F%	2.49

Fig. 4. *In vivo* PK study of VL-MG-9 and CC-885 in C57BL/6 mice (40 mg/kg subcutaneous (S.C.) and 2 mg/kg intravenous (I.V.)) ($n = 3$ mice per group). (A) Semilogarithmic plot of plasma concentration-time curve and PK parameters of VL-MG-9. (B) Semilogarithmic plot of plasma concentration-time curve and PK parameters of CC-885. Blood samples from each group were obtained at 0.0833, 0.25, 0.5, 1, 2, 4, 8, 24 h after administration, and then samples were analyzed by liquid chromatography-mass spectrometry (LC-MS). Data are expressed as the mean ± SD.

In summary, we developed vc-MGs that serves as a novel strategy for the targeted treatment of human B-cell malignancy. Remarkably, the representative compound VL-MG-9, efficiently activated by 430 nm light, could significantly degrade the target protein GSPT1 and inhibit the growth of Burkitt's lymphoma RAMOS cells. Furthermore, the pharmacologic action of VL-MG-9, initiated by visible-light *in vivo*, also resulted in an obvious antitumor effect in mouse xenograft models. Additionally, VL-MG-9 or 430 nm light alone had nearly no protein degradation or general toxicity effects either *in vitro* or *in vivo*, indicating the significant promise for the safety benefits of optical control in biological contexts. More importantly, the PK profiles, including the T_{max}, C_{max} and *F*%, of VL-MG-9 was much better than that of CC-885. These findings demonstrate that vc-MGs exhibit much better druggability in can-

cer treatment *in vivo*. Therefore, our results introduce a novel class of vc-MGs, which exhibit notable advantages over conventional molecular glue CC-885 in terms of efficacy, safety, practicality and druggability, providing a general and powerful photocaged molecular glues strategy for targeted cancer therapy in the future.

Declaration of competing interest

The authors declare that they have no known competing financial interests or personal relationships that could have appeared to influence the work reported in this paper.

CRediT authorship contribution statement

Wei Yan: Writing – original draft, Formal analysis, Data curation, Conceptualization. **Naizhen Zhang:** Writing – original draft, Formal analysis, Data curation. **Xiao Liu:** Writing – original draft, Data curation. **Qiyu He:** Data curation. **Xucheng Lv:** Validation. **Jianghui Sun:** Investigation. **Lili Zhuang:** Investigation. **Yuexin Zou:** Software. **Yajie Zhang:** Software. **Yuhang Liang:** Visualization. **Yanjie Wang:** Methodology. **Siyuan Li:** Methodology. **Yonghui Sun:** Writing – review & editing, Writing – original draft, Visualization, Validation, Supervision, Project administration, Methodology, Investigation, Funding acquisition, Formal analysis, Data curation, Conceptualization.

Acknowledgments

Financial support for this work was sponsored by Beijing Nova Program (No. 20240484709), the National Natural Science Foundation of China (No. 82304315), the Non-profit Central Research Institute Fund of Chinese Academy of Medical Sciences (No. 2023-RC350–02), and Startup Funding from State Key Laboratory of Bioactive Substance and Function of Natural Medicines, Institute of Materia Medica, Chinese Academy of Medical Sciences & Peking Union Medical College.

Supplementary materials

Supplementary material associated with this article can be found, in the online version, at doi:10.1016/j.cclet.2025.112064.

References

[1] C. López, B. Burkhardt, J.K.C. Chan, et al., Nat. Rev. Dis. Primers 8 (2022) 78.
[2] X. Zhu, S. Zhang, Y. Cao, et al., Chin. Chem. Lett. 34 (2023) 108234.
[3] B. Burkhardt, U. Michgehl, J. Rohde, et al., Nat. Commun. 13 (2022) 3881.
[4] K. Dunleavy, S. Pittaluga, M. Shovlin, et al., N. Engl. J. Med 369 (2013) 1915–1925.
[5] F.P. Freitas, H. Alborzinia, A.F. dos Santos, et al., Nature 626 (2024) 401–410.
[6] H. Kretzmer, S.H. Bernhart, W. Wang, et al., Nat. Genet. 47 (2015) 1316–1325.
[7] M. Roschewski, L.M. Staudt, W.H. Wilson, N. Engl. J. Med. 387 (2022) 1111–1122.
[8] E. Campo, Nat. Genet. 44 (2012) 1288–1289.
[9] Q. Zeng, Z. Liu, T. Niu, et al., Chin. Chem. Lett. 34 (2023) 107747.
[10] R. Schmitz, R.M. Young, M. Ceribelli, et al., Nature 490 (2012) 116–120.
[11] J. Xiao, S. Du, G. Dai, et al., Sci. Rep. 7 (2017) 1905.
[12] K. Tomska, R. Kurilov, K.S. Lee, et al., Sci. Rep. 8 (2018) 12046.
[13] J. Li, S.M. Canham, H. Wu, et al., Nat. Chem. Biol. 20 (2024) 365–372.
[14] L. Coelho, K.Oltion Matthew, et al., Nat. Chem. Biol. 20 (2024) 877–884.
[15] Y.D. Li, M.W. Ma, M.M. Hassan, et al., Nat. Chem. Biol. 20 (2024) 1640–1649.
[16] S. Guo, H. Xu, Z. Cheng, et al., Chin. Chem. Lett. 36 (2025) 111022.
[17] K. Baek, B.A. Schulman, Nat. Chem. Biol. 16 (2020) 2–3.
[18] D.E. Bussiere, L. Xie, H. Srinivas, et al., Nat. Chem. Biol. 16 (2020) 15–23.
[19] T. Han, M. Goralski, N. Gaskill, et al., Science 356 (2017) eaal3755.
[20] K. Li, G. Dong, S. Wu, et al., Chin. Chem. Lett. 36 (2025) 110280.
[21] Y. Liu, J. Liang, M. Zheng, et al., Chin. Chem. Lett. 36 (2025) 110317.
[22] M. Słabicki, Z. Kozicka, G. Petzold, et al., Nature 585 (2020) 293–297.
[23] Z. Yang, Y. Sun, Z. Ni, et al., Cell Res. 31 (2021) 1315–1318.
[24] Y. Sun, X. Luo, Z. Yang, et al., Chin. Chem. Lett. 34 (2023) 107924.
[25] L. Zhao, J. Zhao, K. Zhong, et al., Signal Transduct. Target. Ther 7 (2022) 113.
[26] R.S. Sellar, A.S. Sperling, M. Słabicki, et al., J. Clin. Invest. 132 (2022) e153514.
[27] J. Yamamoto, T. Ito, Y. Yamaguchi, et al., Chem. Soc. Rev. 51 (2022) 6234–6250.
[28] B. Hao, X. Li, X. Jia, et al., Acta Pharmacol. Sin. 41 (2020) 1246–1254.
[29] T. Ito, Y. Yamaguchi, H. Handa, Cell Chem. Biol. 28 (2021) 987–999.
[30] Y. Fang, S. Wang, S. Han, et al., Trends Pharmacol. Sci. 44 (2023) 303–317.
[31] T. Asatsuma-Okumura, H. Ando, M. De Simone, et al., Nat. Chem. Biol. 15 (2019) 1077–1084.
[32] M.E. Matyskiela, G. Lu, T. Ito, et al., Nature 535 (2016) 252–257.
[33] C. Surka, L. Jin, N. Mbong, et al., Blood 137 (2021) 661–677.
[34] A. Baradaran-Heravi, A.D. Balgi, S. Hosseini-Farahabadi, et al., Nucleic Acids Res. 49 (2021) 3692–3708.
[35] S. Lier, A. Sellmer, F. Orben, et al., Bioorg. Chem. 119 (2022) 105505.
[36] E.R. Ruskowitz, C.A. DeForest, Nat. Rev. Mater. 3 (2018) 17087.
[37] Y. Fu, N.A. Simeth, W. Szymanski, et al., Nat. Rev. Chem. 8 (2024) 665–685.
[38] K. Elliott, V.K. Singh, M. Boström, et al., Nat. Commun. 14 (2023) 2701.
[39] K. Selvam, S. Sivapragasam, G.M.K. Poon, et al., Nat. Commun. 14 (2023) 2702.
[40] N.K. Sinha, C. McKenney, Z.Y. Yeow, et al., Cell 187 (2024) 3652–3670 e40.
[41] Y. Sun, X. Zhao, N. Ding, et al., Cell Res. 28 (2018) 779–781.
[42] V. Kotla, S. Goel, S. Nischal, et al., J. Hematol. Oncol. 2 (2009) 36.
[43] C.C. Bjorklund, L. Lu, J. Kang, et al., Blood Cancer J. 5 (2015) e354.